Optical interference in view of the probability distribution of photon detection

Toru Kawakubo and Katsuji Yamamoto
Department of Nuclear Engineering, Kyoto University, Kyoto 615-8540, Japan
(Dated: January 3, 2014)

We investigate interference of optical fields by examining the probability distribution of photon detection. The usual description of interference patterns in terms of superposition of classical mean fields with definite phases is elucidated in quantum fashion. Especially, for interference of two independent mixtures of number states with Poissonian or sub-Poissonian statistics, despite lack of intrinsic phases, it is found that the joint probability has a distinct peak manifold in the multi-dimensional space of the detector outcomes, which is along the trajectory of the mean-field values as the relative phase varies on the unit circle. Then, an interference pattern should mostly appear in each shot of measurement as a point in the peak manifold with a randomly chosen relative phase. On the other hand, for super-Poissonian sources the mean-field description is likely invalidated with rather broad probability distributions.

PACS numbers: 42.50.Ar, 42.50.St, 03.65.Ta

arXiv:1401.0436v1 [quant-ph] 2 Jan 2014

I. INTRODUCTION

Interference is often considered as a signature of superposition in quantum systems. In particular, interference in many-body systems as a macroscopic quantum effect has been attracting many interests. In usual experiments, two fields originating in a common source are subject to interfere, namely, each particle interferes with itself [1, 2]. On the other hand, in many-boson systems including lasers [3–5] and atomic Bose-Einstein condensates (BECs) [6], interference has been observed even between independently prepared particles, especially as spatial fringes in a single shot indicating the second-order coherence. Such interference is often explained in terms of the spontaneous symmetry breaking for the relative phase between the independent sources, which presumes nonvanishing expectation values of the field operators or classical mean fields with definite phases. However, the symmetry breaking seems problematic in the absence of real mechanism. In BECs, a U(1) symmetry is relevant for the global phase rotation of atomic wavefunctions, the breakdown of which relies on a nonphysical interaction [7, 8]. In optical systems, a U(1) symmetry is also imposed from lack of an absolute phase reference, which describes the effective photon-number conservation in optical processes [9–11].

The interference pattern observed in a single shot of measurement for independent sources under the U(1) symmetry has been attributed to the back-action of particle detection on the systems, which causes localization of the relative phase [9, 10, 12, 13]. Another approach to the interference is to calculate the correlation functions of the particle numbers measured by the different detectors, which show the spatial modulation. By evaluating the statistical moments of the Fourier components of the spatial modulation up to the fourth order, the plane-wave interference of atomic BECs is predicted in a single run with a random phase [7, 14]. This analysis exploits the nature of the plane-wave mode functions.

In this paper, we investigate the interference of optical fields comprehensively under various configurations for sources and detectors, which is based on the probability theory of quantum measurement. Specifically, we examine the probability distribution of the photon numbers which are registered by the detectors, rather than evaluating the correlation functions of the field intensities as the averages over many runs of measurement. This approach is hence of direct relevance to see the interference pattern in each single shot. Especially, for interference of two independent mixtures of number states, despite lack of intrinsic phases due to the U(1) symmetry, the joint probability in the multi-dimensional space of the photon counts at the detectors may have a distinct manifold of sharp peaks along the trajectory of the mean-field values as the relative phase varies from $-\pi$ to π. Then, the photon-number outcomes in each shot of measurement should mostly be realized as a point in the peak manifold with a randomly chosen relative phase, exhibiting an interference pattern. Hence, the probability distribution of photon detection provides a quantitative criterion to inspect whether an interference pattern appears or not as described with the classical mean fields. We examine the single-shot interference patterns for U(1)-invariant source fields with a variety of photon-number statistics. It will turn out that the mean-field description is applicable to independent fields with Poissonian or sub-Poissonian statistics, whereas for super-Poissonian statistics it is likely invalidated with rather broad probability distributions.

The rest of this paper is presented as follows. In Sec. II, the quantum states of two source fields for interference are described under the U(1) symmetry of phase transformation representing the photon-number superselection rule. In Sec. III, the photon detection for interference is described. A model of photon-detection system is presented. Then, the joint probability of the photon counts at the detectors is given in terms of the mode functions and operators for the source fields. Furthermore, relation among a variety of interference setups is viewed as scaling for detectors and sources. In Sec. IV,

the usual description of interference with classical mean fields is examined in the quantum viewpoint by inspecting the probability distributions of the photon counts. In Sec. V, a detailed numerical analysis is presented to confirm the features of interference which are examined in the preceding sections. Section VI is devoted to conclusion. A derivation of the joint probability of the photon counts is presented in Appendix A.

II. SOURCE FIELDS UNDER PHOTON-NUMBER SUPERSELECTION

We consider a system of optical fields, where two sources are contained for interference, either independent with lack of intrinsic phases or correlated with a definite relative phase. The positive-frequency field operator $\hat{\psi}(\mathbf{x},t)$ is given generally in terms of the annihilation operators $\hat{a}_l$ for a complete set of mode functions ϕ_l:

$$\hat{\psi}(\mathbf{x},t)=\sum_l \hat{a}_l\phi_l(\mathbf{x},t). \tag{1}$$

Here, the time evolution of the free field is represented in the mode functions $\phi_l(\mathbf{x},t)$, which may be determined in practice by expanding $\hat{\psi}$ alternatively in terms of the plane-wave modes. In order to describe an interference experiment, the mode functions are chosen suitably to provide the two source fields as

$$\hat{a}\equiv\hat{a}_1,\hat{b}\equiv\hat{a}_2. \tag{2}$$

For instance, in interference between two wave packets of light the wavevector distributions are localized around the central wavevectors of the respective sources. In the following we assume for simplicity that all the photons are populated in the two source modes ($l=1,2$), while the other modes ($l\geq 3$) are in the vacuum states. This treatment will be almost valid in usual interference experiments.

The quantum systems such as optical fields empirically obey the superselection rule based on the conservation of particles (photons). This is represented by the U(1) symmetry, implying the absence of an absolute phase reference for the Bose fields [11]. Henceforth, we consider the quantum description of interference practically for the U(1)-invariant source fields. The density matrix of each source $\hat{\rho}_s$ ($s=a,b$), respecting the U(1) symmetry, is given by a photon-number distribution $p_s(N)$ for a mixture of the number states, or a phase-invariant coherent-state representation $\mathcal{P}_s(|\alpha|)$ ($\alpha\equiv r_s e^{i\phi_s}$) [10]:

$$\begin{aligned}\hat{\rho}_s&=\sum_{N=0}^{\infty}p_s(N)|N\rangle\langle N|=\int\frac{d^2\alpha}{2\pi}\mathcal{P}_s(|\alpha|)|\alpha\rangle\langle\alpha|\\&\equiv\int_{-\pi}^{\pi}\frac{d\phi_s}{2\pi}\int_0^{\infty}r_s dr_s\mathcal{P}_s(r_s)|r_s e^{i\phi_s}\rangle\langle r_s e^{i\phi_s}|.\end{aligned} \tag{3}$$

For example, a Poissonian source $\hat{\Pi}(|\alpha|)$ with a mean photon number $\bar{N}=|\alpha|^2$ is specified as

$$p(N;\hat{\Pi})=e^{-\bar{N}}\frac{\bar{N}^N}{N!}, \tag{4}$$

$$\mathcal{P}(r;\hat{\Pi})=2\delta(r^2-\bar{N}), \tag{5}$$

$$\hat{\Pi}(|\alpha|)=\int_{-\pi}^{\pi}\frac{d\phi}{2\pi}|\sqrt{\bar{N}}e^{i\phi}\rangle\langle\sqrt{\bar{N}}e^{i\phi}|. \tag{6}$$

The state of two independent sources is then given by

$$\hat{\rho}_{a\otimes b}\equiv\hat{\rho}_a\otimes\hat{\rho}_b, \tag{7}$$

with the uncorrelated random phases ϕ_a and ϕ_b under the U(1) symmetry.

On the other hand, the two fields may originate in a common U(1)-invariant source. By denoting the operators $\hat{c}_1$ and $\hat{c}_2$, respectively, for the original source mode and the orthogonal auxiliary mode in the vacuum, the operators for the two source fields may be given in terms of a unitary transformation,

$$\begin{pmatrix}\hat{a}\\ \hat{b}\end{pmatrix}=\begin{pmatrix}c & -se^{-i\delta}\\ se^{i\delta} & c\end{pmatrix}\begin{pmatrix}\hat{c}_1\\ \hat{c}_2\end{pmatrix}, \tag{8}$$

where $0\leq s,c\leq 1$, $s^2+c^2=1$, and δ is a certain given phase. Then, an original number state $|N\rangle_1$ provides entangled sources preserving the U(1) symmetry as

$$\begin{aligned}|N\rangle_1|0\rangle_2&=\frac{(c\hat{a}^\dagger+se^{i\delta}\hat{b}^\dagger)^N}{\sqrt{N!}}|0\rangle_1|0\rangle_2\\&=\sum_{K=0}^{N}\frac{\sqrt{N!}}{\sqrt{K!}\sqrt{(N-K)!}}c^K s^{N-K}e^{i(N-K)\delta}\\&\quad\times|K\rangle_a|N-K\rangle_b.\end{aligned} \tag{9}$$

A common Poissonian state $\hat{\Pi}_1(|\alpha|)$ ($\alpha\equiv|\alpha|e^{i\phi}$) also provides

$$\begin{aligned}&\int_{-\pi}^{\pi}\frac{d\phi}{2\pi}(|\alpha\rangle\langle\alpha|)_1\otimes(|0\rangle\langle 0|)_2\\&=\int_{-\pi}^{\pi}\frac{d\phi}{2\pi}(|c\alpha\rangle\langle c\alpha|)_a\otimes(|se^{i\delta}\alpha\rangle\langle se^{i\delta}\alpha|)_b,\end{aligned} \tag{10}$$

where the resultant two sources share the original random phase ϕ, and develop the definite relative phase δ. The fields from a general common source $\hat{\rho}_1^{\rm com}$ are represented in terms of the states given in the above with the original $p(N)$ or U(1)-invariant $\mathcal{P}(|\alpha|)$ for $\hat{\rho}_1^{\rm com}$.

Furthermore, if the two sources can refer to a certain frame system for specifying their relative phase δ, they may be represented in the U(1)-invariant form as

$$\begin{aligned}\hat{\rho}_{ab}(\delta)\equiv&\int_{-\pi}^{\pi}\frac{d\phi}{2\pi}\int_0^{\infty}r_a dr_a\mathcal{P}_a(r_a)\int_0^{\infty}r_b dr_b\mathcal{P}_b(r_b)\\&\times|r_a e^{i(\phi+\delta)}\rangle\langle r_a e^{i(\phi+\delta)}|\otimes|r_b e^{i\phi}\rangle\langle r_b e^{i\phi}|.\end{aligned} \tag{11}$$

The state of independent sources in Eq. (7) is then given formally as

$$\hat{\rho}_{a\otimes b}=\int_{-\pi}^{\pi}\frac{d\delta}{2\pi}\hat{\rho}_{ab}(\delta), \tag{12}$$

which is the average over the random relative phase δ.

III. PHOTON DETECTION FOR INTERFERENCE

A. Photon detection and probability distribution

In optical interference experiments, a commonly used photodetector records the number of photoelectrons emitted from the detector surface during a time interval T. The time and surface integrated photon-flux operator for the electron emission at some detector m is given [15–18] by

$$\hat{I}_m = \eta_m \int_0^T dt \int_{S_m} dxdy \hat{\psi}^\dagger(\mathbf{x},t)\hat{\psi}(\mathbf{x},t), \tag{13}$$

where η_m is the quantum efficiency, and the z axis is taken normal to the detector surface S_m. The bandwidth $\Delta\omega$ of the incident radiation is assumed to be small enough compared with the central frequency ω_0. The photon-flux operators in Eq. (13) may be expressed as bilinear forms of the mode operators,

$$\hat{I}_m = \sum_{ll'} R^{(m)}_{ll'} \hat{a}^\dagger_l \hat{a}_{l'}, \tag{14}$$

where the Hermitian matrices $R^{(m)}$ are obtained from Eq. (13) by substitution $\hat{\psi}^\dagger\hat{\psi} \to \phi^*_l\phi_{l'}$ as

$$R^{(m)}_{ll'} = \eta_m \int_0^T dt \int_{S_m} dxdy \phi^*_l(\mathbf{x},t)\phi_{l'}(\mathbf{x},t). \tag{15}$$

The joint probability of the photon counts $n_1,\ldots,n_M \equiv \mathbf{n}_M$ registered by the M detectors, which characterizes the statistics of interference, is given [15–18] by

$$\begin{aligned} P(n_1,\ldots,n_M) &\equiv P(\mathbf{n}_M) \\ &= \mathrm{Tr}\left[\hat{\rho} : \prod_{m=1}^M \frac{(\hat{I}_m)^{n_m}}{n_m!} e^{-\hat{I}_m} :\right], \end{aligned} \tag{16}$$

where : : stands for normal ordering. (A derivation is presented in Appendix A.) Then, the reduction relation follows as

$$P(\mathbf{n}_{M-1}) = \sum_{n_M} P(\mathbf{n}_M). \tag{17}$$

The joint probability is also additive for a combination of source states as

$$\hat{\rho} = \sum_{i=1}^K c_i\hat{\rho}_i \to P(\mathbf{n}_M) = \sum_{i=1}^K c_i P_i(\mathbf{n}_M), \tag{18}$$

where $c_1+\cdots+c_K = 1$ $(0 < c_i \le 1)$. The flux operators are given specifically as

$$\hat{I}_m = R^{(m)}_{aa}\hat{a}^\dagger\hat{a} + R^{(m)}_{bb}\hat{b}^\dagger\hat{b} + R^{(m)}_{ab}\hat{a}^\dagger\hat{b} + R^{(m)}_{ba}\hat{b}^\dagger\hat{a}, \tag{19}$$

where $R^{(m)}_{aa}, R^{(m)}_{bb} > 0$, and

$$R^{(m)}_{ab} = R^{(m)*}_{ba} \equiv \xi_m e^{i\theta_m}\sqrt{R^{(m)}_{aa}R^{(m)}_{bb}}, \tag{20}$$

with a certain phase θ_m and $0 \le \xi_m \le 1$, representing the visibility of interference pattern, in accordance with the Cauchy-Schwartz inequality for Eq. (15). It should be noted that the terms involving the vacuum modes ($l \ge 3$) are dropped in $\hat{I}_m$ since they provide null contributions to Eq. (16) as the normal-ordered expectation values. The maximal visibility parameter $\xi_m = 1$ may usually be obtained by a suitable detection system, where the variation of the relative phase between the mode functions, $\arg[\phi^*_a(\mathbf{x})\phi_b(\mathbf{x})] \approx \theta_m$, is negligible on the detector surface S_m (e.g., the sources being apart sufficiently from the detectors), together with $\phi_{a,b}(\mathbf{x},t) \approx \phi_{a,b}(\mathbf{x})e^{-i\omega_0 t}$ for the quasi-monochromatic modes ($\Delta\omega \ll \omega_0$). In this situation, the detector matrices representing the flux operators in Eq. (15) may be factorized approximately in terms of the stationary mode functions as

$$R^{(m)}_{ll'} \approx \kappa_m \phi^*_l(\mathbf{x}_m)\phi_{l'}(\mathbf{x}_m), \tag{21}$$

where $\mathbf{x}_m \in S_m$ and $\kappa_m = \eta_m T|S_m|$ with the detection area $|S_m|$. Then, the flux-operator is expressed as

$$\hat{I}_m = \kappa_m \hat{\Psi}^\dagger_m \hat{\Psi}_m, \tag{22}$$

with a superposition of the mode operators,

$$\hat{\Psi}_m = \phi_{ma}\hat{a} + \phi_{mb}\hat{b}, \tag{23}$$

where $\phi_{ma} \equiv \phi_a(\mathbf{x}_m)$ and $\phi_{mb} \equiv \phi_b(\mathbf{x}_m)$.

B. Scaling for detectors and sources

For the two independent U(1)-invariant sources $\hat{\rho} = \hat{\rho}_{a\otimes b}$ in Eq. (7), the mean photon number measured at each detector is given by

$$\begin{aligned} \langle n_m\rangle &= \mathrm{Tr}[\hat{\rho}_{a\otimes b}\hat{I}_m] \\ &= R^{(m)}_{aa}\bar{N}_a + R^{(m)}_{bb}\bar{N}_b \\ &\equiv \langle n_m\rangle_a + \langle n_m\rangle_b, \end{aligned} \tag{24}$$

with the mean photon numbers $\bar{N}_s = \mathrm{Tr}[\hat{\rho}_s\hat{s}^\dagger\hat{s}]$ initially contained in the sources. The interference term with $R^{(m)}_{ab} = R^{(m)*}_{ba}$, indicating the so-called second-order coherence, disappears in Eq. (24) on average over many runs of measurement. It, however, will be seen later in detail that the interference fringes may arise in each shot [3] as the outcomes $\{n_m\}$ of photon detection, which are obtained according to the joint probability in Eq. (16).

We note in Eq. (24) that the coefficients $R^{(m)}_{aa}$ and $R^{(m)}_{bb}$ indicate the probabilities for each photon from the respective sources to fall into detector m. They may represent the resolution of interference. Specifically, $R^{(m)}_{ss} \propto |S_m|$ decreases as $1/M \to 0$, but keeping

$\langle n_m\rangle_s = R^{(m)}_{ss}\bar{N}_s \gg 1$ for high accuracy statistics, when the photons are measured by continuously distributed many small detectors ($M \gg 1$), resulting in a fine spatial interference fringes. In this sense, as seen in Eq. (24), a change of $R^{(m)}_{ss}$ (or resolution) for the detectors may be viewed alternatively as an modification of the source statistics. Here, consider scaling of the detector matrices $R^{(m)}$ (by change of the detection efficiencies $\kappa_m = \eta_m T|S_m|$),

$$\tilde{R}^{(m)}(q) = R^{(m)}/q \qquad (q > 0), \tag{25}$$

and define the binomial distribution

$$B^N_{N'}(q) \equiv \binom{N}{N'} q^{N'}(1-q)^{N-N'} \quad (0 \le N' \le N). \tag{26}$$

In evaluating the joint probability, $\langle:(\hat{I}_1)^{k_1}\cdots(\hat{I}_M)^{k_M}:\rangle$ contained in Eq. (16) are calculated for a number state $|N_a, N_b\rangle$ with the normal-ordered expectation values $\langle(\hat{b}^\dagger)^{k_b}(\hat{a}^\dagger)^{k_a}\hat{a}^{k_a}\hat{b}^{k_b}\rangle = [N_a!/(N_a-k_a)!]\times[N_b!/(N_b-k_b)!]$ $(k_a + k_b = k_1 + \cdots + k_M)$, which are multiplied by $q^{k_a}q^{k_b}$ under the scaling. Then, by considering the relation $q^k[N!/(N-k)!] = \sum_{N'=k}^N B^N_{N'}(q)[N'!/(N'-k)!]$, the effects of this scaling can be included in the source statistics without changing the calculations in Eq. (16) as

$$\tilde{p}_s(N;q) = \sum_{N'=N}^{\infty} p_s(N')B^{N'}_N(q), \tag{27}$$

which is also normalized as the original $p_s(N)$. Hence, the number statistics of the sources may be replaced with the effective ones in Eq. (27) by the scaling of q, reproducing the same joint probability:

$$\{\tilde{R}^{(m)}(q), \tilde{p}_s(N;q)\} \to P(\mathbf{n}_M). \tag{28}$$

This may be viewed as a renormalization transformation among the number statistics. It indicates intimate relation for interference phenomena in a variety of setups for detectors and sources. According to Eq. (27), the mean $\tilde{\bar{N}}_s$ and variance $\tilde{V}_s$ for the effective statistics are given in terms of the original ones as

$$\tilde{\bar{N}}_s = q\bar{N}_s, \tag{29}$$

$$\tilde{V}_s = q^2V_s + (1-q)q\bar{N}_s, \tag{30}$$

preserving $\tilde{R}^{(m)}\tilde{\bar{N}}_s = R^{(m)}\bar{N}_s$. Then, for a sub-Poissonian distribution ($V_s < \bar{N}_s$), the effective one is still sub-Poissonian ($\tilde{V}_s < \tilde{\bar{N}}_s$) as

$$\tilde{V}_s/\tilde{\bar{N}}_s = q(V_s/\bar{N}_s) + 1 - q. \tag{31}$$

The Poissonian form is preserved under the renormalization up to the scaling of the mean as $\tilde{\bar{N}}_s = q\bar{N}_s$. On the other hand, for a super-Poissonian distribution the effective one is still super-Poissonian.

IV. MEAN-FIELD DESCRIPTION

The interference pattern is usually described with superposition of classical mean fields. We here consider quantum theoretical reasoning of this picture. In the mean-field description, the source-mode operators are replaced with c-number complex amplitudes as $\hat{a} \to \alpha$ and $\hat{b} \to \beta$. That is, the physical quantities in normal ordering are evaluated as the expectation values for coherent states $|\alpha,\beta\rangle \equiv |\alpha\rangle_a|\beta\rangle_b$ with definite phases. Then, the mean photon-number count at each detector is given by

$$\begin{aligned}\bar{n}_m(\delta) &= \langle\alpha,\beta|\hat{I}_m|\alpha,\beta\rangle \\ &= \langle n_m\rangle_a + \langle n_m\rangle_b \\ &\quad +2\xi_m\sqrt{\langle n_m\rangle_a\langle n_m\rangle_b}\cos(\delta+\theta_m),\end{aligned} \tag{32}$$

where $\delta = \arg\alpha - \arg\beta$, $|\alpha|^2 = \bar{N}_a$, $|\beta|^2 = \bar{N}_b$, $\langle n_m\rangle_a = R^{(m)}_{aa}\bar{N}_a$ and $\langle n_m\rangle_b = R^{(m)}_{bb}\bar{N}_b$ as given in Eq. (24) for the two independent U(1)-invariant sources. The set of $\{\bar{n}_m(\delta)\}$ with the definite relative phase δ exhibits the interference pattern with the cosine term in Eq. (32), which oscillates with θ_m depending on the detector location. Specifically for the usual case with $\xi_m = 1$ of maximal visibility, Eqs. (21), (22) and (23) for $R^{(m)}_{ll'}$ and $\hat{I}_m$ provide the interference pattern in terms of the superposition of the macroscopic wavefunctions $\alpha\phi_a$ and $\beta\phi_b$ of the two source modes:

$$\bar{n}_m(\delta) = \kappa_m\left|\alpha\phi_a(\mathbf{x}_m) + \beta\phi_b(\mathbf{x}_m)\right|^2. \tag{33}$$

We note in Eqs. (20), (24), (29) and (32) that ξ_m, θ_m, $\langle n_m\rangle_a$, $\langle n_m\rangle_b$, and hence the mean-field description $\bar{n}_m(\delta)$ is invariant under the q-scaling in Eq. (28).

The joint probability of photon detection in Eq. (16) is calculated with $\langle\alpha,\beta|:(\hat{I}_m)^k:|\alpha,\beta\rangle = [\bar{n}_m(\delta)]^k$ $(k \ge 0)$ for the mean-field description as

$$\begin{aligned}P(\mathbf{n}_M;\delta) &= \prod_{m=1}^M \frac{[\bar{n}_m(\delta)]^{n_m}}{n_m!}e^{-\bar{n}_m(\delta)} \\ &\equiv \prod_{m=1}^M P(n_m;\delta).\end{aligned} \tag{34}$$

This is the product of the Poisson distributions $P(n_m;\delta)$ at the respective detectors. Hence, the interference pattern appears for the outcomes in each shot of measurement as $\{n_m\} \approx \{\bar{n}_m(\delta)\}$ with the shot noise $\Delta n_m = \sqrt{\bar{n}_m}$.

The mean-field description is, however, not directly applicable to the independent U(1)-invariant sources in Eq. (7) with $\mathrm{Tr}[\hat{\rho}_{a\otimes b}\hat{a}^\dagger\hat{b}] = \mathrm{Tr}[\hat{\rho}_a\hat{a}^\dagger]\times\mathrm{Tr}[\hat{\rho}_b\hat{b}] = 0$, eliminating the cosine term in Eq. (32):

$$\langle n_m\rangle = \langle n_m\rangle_a + \langle n_m\rangle_b \neq \bar{n}_m(\delta). \tag{35}$$

Nevertheless, by experiments and theoretical calculations the interference fringes are observed for Poissonian sources (laser fields [3]) and sub-Poissonian sources (optical number states [9, 10] and BECs [6, 7, 12–14]). In

the following, we examine the validity of the mean-field description for a variety of source fields under the U(1) symmetry.

A. Poissonian sources and the peak manifold of the joint probability distribution

We first consider as a prototype the case of two independent Poissonian sources,

$$\hat{\rho}_{a\otimes b} = \hat{\Pi}_a \otimes \hat{\Pi}_b = \int_{-\pi}^{\pi} \frac{d\phi}{2\pi} \int_{-\pi}^{\pi} \frac{d\delta}{2\pi} |\alpha,\beta\rangle\langle\alpha,\beta|, \quad (36)$$

where $\arg\alpha = \phi + \delta$ and $\arg\beta = \phi$. The joint probability of photon detection for these Poissonian sources is given according to the additivity in Eq. (18) by

$$P_{\hat{\Pi}}(\mathbf{n}_M) \equiv P(\mathbf{n}_M; \hat{\Pi}_a \otimes \hat{\Pi}_b) = \int_{-\pi}^{\pi} \frac{d\delta}{2\pi} P(\mathbf{n}_M;\delta). \quad (37)$$

This is the average of the mean-field description $P(\mathbf{n}_M;\delta)$ in Eq. (34) over the intrinsically random and unknown relative phase δ under the U(1) symmetry representing the photon-number superselection rule. It is considered here that $\bar{n}_m(\delta)$ for $P(\mathbf{n}_M;\delta)$ is independent of the overall phase ϕ. Even though the second-order coherence is not observed manifestly in Eq. (24), the form of the joint probability such as $P(\mathbf{n}_M;\hat{\Pi}_a \otimes \hat{\Pi}_b)$ in Eq. (37) indicates the interference effects between the two independent fields, which may be observed as the single-shot interference patterns and intensity correlations. This is readily seen as follows. Note that each $P(\mathbf{n}_M;\delta)$ in Eq. (34) for the coherent states with a relative phase δ has a sharp peak at the point $\{\bar{n}_m(\delta)\}$ ($\bar{n}_m(\delta) \gg 1$) in the M-dimensional space of the photon counts $\mathbf{n}_M$. Then, Eq. (37) implies that there exists the manifold of these peaks along the closed trajectory of the mean-field values, practically providing the support of $P_{\hat{\Pi}}(\mathbf{n}_M)$:

$$\mathrm{supp}[P_{\hat{\Pi}}(\mathbf{n}_M)] \approx \{\bar{n}_m(\delta)\}(\delta : -\pi \to \pi). \quad (38)$$

According to this specific form of the joint probability $P_{\hat{\Pi}}(\mathbf{n}_M)$, the actual outcomes $\{n_m\}$ are mostly realized as a point in the peak manifold with some relative phase δ_1 randomly chosen a posteriori:

$$\{n_m\} \approx \{\bar{n}_m(\delta_1)\}. \quad (39)$$

Therefore, an interference pattern is exhibited in each shot of measurement as described with the mean fields.

In comparison, the photon detection may be made sequentially first for the source $\hat{\rho}_a$, and then after a time interval for the source $\hat{\rho}_b$. For these two entirely separate sources without any coherence, interference by no means occurs between them. The total joint probability for these subsequent measurements is given by combining incoherently the individual joint probabilities P_a for $\hat{\rho}_a$ and P_b for $\hat{\rho}_b$:

$$P^{\mathrm{incoh}}(\mathbf{n}_M) = \sum_{\mathbf{n}'_M} P_a(\mathbf{n}'_M) P_b(\mathbf{n}_M - \mathbf{n}'_M). \quad (40)$$

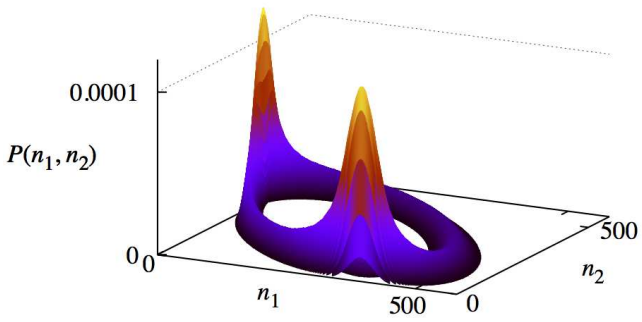

FIG. 1. (Color online) The joint probability $P(n_1, n_2)$ is depicted for the Poissonian sources $\hat{\Pi}_a \otimes \hat{\Pi}_b$ with $\bar{N}_a = \bar{N}_b = 500$. The peak manifold of $P(n_1, n_2)$ exists along the mean-field trajectory $\{\bar{n}_1(\delta), \bar{n}_2(\delta)\}(\delta : -\pi \to \pi)$. The conditional distribution $P^{\mathrm{c}}(n_2|n_1)$, up to the normalization, provides a cross section of the peak manifold.

This incoherent joint probability is calculated explicitly for the pair of $\hat{\Pi}_a$ and $\hat{\Pi}_b$ as

$$P^{\mathrm{incoh}}_{\hat{\Pi}}(\mathbf{n}_M) \propto \prod_{m=1}^{M} \frac{[\langle n_m\rangle_a + \langle n_m\rangle_b]^{n_m}}{n_m!}, \quad (41)$$

which merely has a single peak in the $\mathbf{n}_M$ space at the point $\{\langle n_m\rangle_a + \langle n_m\rangle_b\}$ without the interference term, in contrast with $P_{\hat{\Pi}}(\mathbf{n}_M)$.

The feature of the joint probability $P(\mathbf{n}_M)$ for the Poissonian sources $\hat{\Pi}_a \otimes \hat{\Pi}_b$ with $\bar{N}_a = \bar{N}_b = 500$, as given in Eq. (37), is depicted on the (n_1, n_2) plane in Fig. 1, where the detector matrices $R^{(m)}$ are taken typically as in Eq. (58) (see Sec. V). The peak manifold of $P(n_1, n_2)$ appears clearly along the mean-field trajectory $\{\bar{n}_1(\delta), \bar{n}_2(\delta)\}(\delta : -\pi \to \pi)$ as given in Eq. (32). In this case with $\sqrt{\langle n_m\rangle_a} \approx \sqrt{\langle n_m\rangle_b}$ ($R^{(m)}_{aa}\bar{N}_a \sim R^{(m)}_{bb}\bar{N}_b$) and $\xi_m = 1$ for the maximal visibility ($m = 1, 2$), the two prominent peaks are particularly seen in the regions corresponding, respectively, to $\bar{n}_1(\delta_1) \ll \langle n_1\rangle$ and $\bar{n}_2(\delta_2) \ll \langle n_2\rangle$ for certain δ_1 and δ_2 satisfying $\cos(\delta_m + \theta_m) = -1$. The peak manifold becomes rather thin there, and the probability distribution is squeezed along the n_m direction with the narrow width $\sqrt{\bar{n}_m(\delta_m)}$ of the Poisson distribution $P(n_m;\delta_m)$ for the specific δ_m. That is, the peak is enhanced by a factor $\sim \sqrt{\langle n_m\rangle}/\sqrt{\bar{n}_m(\delta_m)}$ (numerically about 3 here). The probability for the interference pattern to be realized within the area $\sqrt{\langle n_1\rangle}\sqrt{\langle n_2\rangle}$ of the mean shot-noise level is, however, roughly uniform along the peak manifold. If there is a large difference between the source photon numbers as $\bar{N}_a \gg \bar{N}_b$ or $\bar{N}_a \ll \bar{N}_b$, the mean-field trajectory $\{\bar{n}_m(\delta)\}(\delta : -\pi \to \pi)$ shrinks as $2\sqrt{\langle n_m\rangle_a\langle n_m\rangle_b} < \langle n_m\rangle_a + \langle n_m\rangle_b$ in Eq. (32), reducing effectively the visibility of the interference patterns.

B. The conditional distributions and estimation of the relative phase

In order to check more closely the structure of the probability distribution of photon detection for interference, we note that despite lack of intrinsic phases due to the U(1) symmetry, the outcomes at the detectors may provide estimation of the relative phase. Specifically, we examine the conditional distributions of the photon count at a detector given the outcomes at some other detectors.

The conditional distribution $P^{\rm c}(n_2|n_1)$ of the count n_2 at detector 2 with the outcome n_1 at detector 1 is given by

$$P^{\rm c}(n_2|n_1) = \frac{P(n_1,n_2)}{P(n_1)}, \tag{42}$$

which provides a cross section of the peak manifold of the joint probability $P(n_1,n_2)$ in Fig. 1, up to the normalization with $P(n_1)$. By fitting the outcome n_1 to the mean-field value $\bar{n}_1(\delta)$ in Eq. (32), an estimate of the relative phase δ is obtained, generally with two possibilities $\delta^{\pm}$ due to the cosine. Then, the outcome n_2 is inferred with the estimated phases as

$$n_1 = \bar{n}_1(\delta) \to \delta^{\pm}(n_1) \to \bar{n}_2^{\pm} \equiv \bar{n}_2[\delta^{\pm}(n_1)]. \tag{43}$$

Actually, if $P^{\rm c}(n_2|n_1)$ has the sufficiently narrow peaks at $\bar{n}_2^+$ and $\bar{n}_2^-$, the outcome n_2 should be obtained almost at either of these peaks with high probability, as predicted by the mean-field description. The width of each peak should be at most of the order of $\sqrt{\bar{n}_2}$, the shot noise level of the Poisson distribution $P(n_2;\delta) = e^{-\bar{n}_2}(\bar{n}_2)^{n_2}/n_2!$, in order to obtain the interference pattern.

Furthermore, we consider the conditional distribution of the count n_3 at detector 3 for the pair of the outcomes (n_1,n_2),

$$P^{\rm c}(n_3|n_1,n_2) = \frac{P(n_1,n_2,n_3)}{P(n_1,n_2)}. \tag{44}$$

Given the outcome at detector 1 as $n_1 = \bar{n}_1(\delta^{\pm})$, the outcome at detector 2 will mostly be obtained as either $n_2 \approx \bar{n}_2^+ \equiv \bar{n}_2[\delta^+(n_1)]$ or $n_2 \approx \bar{n}_2^- \equiv \bar{n}_2[\delta^-(n_1)]$, completing the estimation of the relative phase $\delta = \delta^+$ or $\delta = \delta^-$. Then, if $P^{\rm c}(n_3|n_1,n_2)$ of n_3 with $n_1 = \bar{n}_1(\delta^{\pm})$ and $n_2 \approx \bar{n}_2^{\pm}$ has a single peak at $\bar{n}_3^{\pm} \equiv \bar{n}_3[\delta^{\pm}(n_1)]$ for either δ^+ or δ^-, the interference pattern mostly appears as $\{\bar{n}_1(\delta^+),\bar{n}_2(\delta^+),\bar{n}_3(\delta^+)\}$ or $\{\bar{n}_1(\delta^-),\bar{n}_2(\delta^-),\bar{n}_3(\delta^-)\}$ according to the mean-field description.

Typically for the independent Poissonian sources $\hat{\Pi}_a \otimes \hat{\Pi}_b$ in Eq. (36), it is expected from Eq. (37) that the conditional distributions behave as

$$P^{\rm c}_{\hat{\Pi}}(n_2|\bar{n}_1) \approx C_+ P(n_2;\delta^+) + C_- P(n_2;\delta^-), \tag{45}$$

with certain normalization factors $C_{\pm} \approx 1/2$, and

$$P^{\rm c}_{\hat{\Pi}}(n_3|\bar{n}_1,\bar{n}_2^{\pm}) \approx P(n_3;\delta^{\pm}). \tag{46}$$

These observations on the conditional distributions confirm that the joint probability $P_{\hat{\Pi}}(\mathbf{n}_{\rm M})$ has the peak manifold in Eq. (38) for the interference patterns, as seen in Fig. 1 for $P_{\hat{\Pi}}(n_1,n_2)$.

C. Sub-Poissonian sources

We next argue that sub-Poissonian sources lead to the narrower peaks in the probability distributions than the Poissonian sources. It is pointed out [19] that wave packets emitted from a cavity maintain a pronounced relative phase coherence when the intracavity field has a narrow number distribution. Light beams from such sub-Poissonian cavities will also exhibit the single-shot interference patterns $\{n_m\} \approx \{\bar{n}_m(\delta)\}$ $(-\pi \le \delta < \pi)$ as given by the mean-field description. This phase coherence of each source is essential to fix the interference phase between the independent sources through the photon detection.

Specifically, consider two independent number states

$$\hat{\rho}_{a\otimes b} = \hat{N}_a \otimes \hat{N}_b \equiv |N_a,N_b\rangle\langle N_a,N_b|. \tag{47}$$

Since the Poissonian states $\hat{\Pi}_a \otimes \hat{\Pi}_b$ are given in terms of the number states $\hat{N}_a \otimes \hat{N}_b$ with the relevant photon-number distributions, we have the relation between the joint probabilities for these source states as

$$P_{\hat{\Pi}}(\mathbf{n}_M) = \sum_{N_a,N_b} p(N_a;\hat{\Pi}_a)p(N_b;\hat{\Pi}_b)P_{\hat{N}}(\mathbf{n}_M). \tag{48}$$

The Poissonian fluctuations of the photon numbers in $p(N_a;\hat{\Pi}_a)$ and $p(N_b;\hat{\Pi}_b)$ will broaden the distribution of the outcomes $\mathbf{n}_M$ to some extent from $P_{\hat{N}}(\mathbf{n}_M)$. Hence, it is inferred by consistency that $P_{\hat{N}}(\mathbf{n}_M)$ should also have the peak manifold of the mean-field description $\{\bar{n}_m(\delta)\}(\delta : -\pi \to \pi)$ with $|\alpha|^2 = N_a$ and $|\beta|^2 = N_b$ in Eq. (32), the width of which is narrower (smaller shot noise) than the Poissonian $P_{\hat{\Pi}}(\mathbf{n}_M)$ as

$$(\Delta n_m)_{\hat{N}} = \gamma\sqrt{\bar{n}_m} \qquad (0<\gamma<1). \tag{49}$$

Generally, the independent fields $\hat{\rho}_a \otimes \hat{\rho}_b$ are represented in terms of either the number states or the coherent states in Eq. (3). The continuously distributed photon-number statistics of the sources with variances $\sim (\Delta N)^2$ broaden the probability distribution, causing dispersion of the mean-field value $\bar{n}_m(\delta)$ as a significant contribution to Eq. (49) for the shot noise. Since the mean-field value depends on the source photon numbers roughly as $\bar{n}_m \sim R\bar{N}$ for $R_{ss}^{(m)} \sim R$ and $\bar{N}_s \sim \bar{N}$ $(s=a,b)$, the shot noise, or the width of the probability distribution of photon detection, is estimated for $\hat{\rho}_a \otimes \hat{\rho}_b$ as

$$(\Delta n_m)_{a\otimes b} \sim \gamma\sqrt{\bar{n}_m} + (\bar{n}_m/\bar{N})\Delta N. \tag{50}$$

Particularly, $(\Delta n_m)_{\hat{\Pi}} = \sqrt{\bar{n}_m}$ implies $1-\gamma \sim \sqrt{\bar{n}_m/\bar{N}}$ with $\Delta N = \sqrt{\bar{N}}$. Here, it should be remarked that the shot noise for the interference of independent sources is not simply estimated with the expectation values (statistical averages) of the moments of the photon-flux operator $\hat{I}_m$ $(\kappa_m \hat{\Psi}_m^\dagger \hat{\Psi}_m)$. This is due to the fact that the

interference patterns vary run by run with randomly chosen relative phases.

We also present an example of discrete photon-number distribution for the sources, where the above estimate of the shot noise in Eq. (50) is not applicable simply. That is, consider certain independent sources such as

$$\hat{\rho}_a \otimes \hat{\rho}_b = \frac{1}{4}(\hat{N}_a^+ + \hat{N}_a^-) \otimes (\hat{N}_b^+ + \hat{N}_b^-) = \frac{1}{4}\sum_{\sigma,\sigma'=\pm} \hat{N}_a^\sigma \otimes \hat{N}_b^{\sigma'}, \quad (51)$$

which are the mixtures of two number states

$$\hat{N}^\pm \equiv |\bar{N} \pm \Delta N\rangle\langle \bar{N} \pm \Delta N|. \quad (52)$$

The mixed state $(\hat{N}^+ + \hat{N}^-)/2$ is the U(1)-invariant form of $(|\bar{N} + \Delta N\rangle + |\bar{N} - \Delta N\rangle)/\sqrt{2}$. It has the variance of photon number $V = (\Delta N)^2$. In particular for the significant number difference with $\Delta N \sim \bar{N}/2$, there are four peak manifolds of $\{\bar{n}_m^{\pm\pm}(\delta)\}$, respectively, for $\hat{N}_a^\pm \otimes \hat{N}_b^\pm$ ($\sigma = \pm$, $\sigma' = \pm$), which are mostly separated in the $\mathbf{n}_M$ space. Any one of these interference patterns appears randomly run by run with the shot noise $\sqrt{\bar{n}_m^{\pm\pm}}$. Hence, the mixed state $(\hat{N}^+ + \hat{N}^-)/2$ is regarded as sub-Poissonian in spite of the apparent large variance $(\Delta N)^2 \sim (\bar{N}/2)^2$ since its photon-number distribution is essentially narrow. The peak manifolds $\{\bar{n}_m^{++}(\delta)\}$ and $\{\bar{n}_m^{--}(\delta)\}$ are similar to each other, providing the same interference pattern with contrast in brightness by the factor $\bar{n}_m^{++}/\bar{n}_m^{--} = (\bar{N} + \Delta N)/(\bar{N} - \Delta N)$. On the other hand, the peak manifolds $\{\bar{n}_m^{+-}(\delta)\}$ and $\{\bar{n}_m^{-+}(\delta)\}$ represent the same interference pattern for $R_{aa}^{(m)} = R_{bb}^{(m)}$.

D. Super-Poissonian sources

As for super-Poissonian sources, they are given relevantly in the coherent-state representation with U(1)-invariant non-singular $\mathcal{P}$ functions. Then, the joint probability of photon detection is given as

$$P_{\mathrm{sup}\hat{\Pi}}(\mathbf{n}_M) = \int_{-\pi}^{\pi} \frac{d\delta}{2\pi} P_{\mathrm{sup}\hat{\Pi}}(\mathbf{n}_M; \delta), \quad (53)$$

where

$$P_{\mathrm{sup}\hat{\Pi}}(\mathbf{n}_M; \delta) = \int_0^\infty \frac{dr_a^2}{2}\mathcal{P}_a(r_a) \int_0^\infty \frac{dr_b^2}{2}\mathcal{P}_b(r_b) \times P(\mathbf{n}_M; \delta; r_a, r_b), \quad (54)$$

with $|\alpha| = r_a$ and $|\beta| = r_b$ for $\bar{n}_m(\delta; r_a, r_b)$ in Eq. (32). Then, typically for thermal fields $\hat{\Theta}_a \otimes \hat{\Theta}_b$ with $\mathcal{P}_s(r_s; \hat{\Theta}_s) \propto \exp(-r_s^2/\bar{N}_s)$, the peak of $P(\mathbf{n}_M; \delta)$ is smeared out in Eq. (54) for each δ, providing the large shot noise $(\Delta n_m)_{\hat{\Theta}} \sim \bar{n}_m$ with $\Delta N \approx \bar{N}$ in Eq. (50). Hence, the interference pattern does not arise anyway for independent super-Poissonian sources such as thermal states, even though the outcomes after many runs of measurement may manifest the higher-order coherence effects, including the correlation of the photon counts.

E. Correlated sources with a definite relative phase

The usual interference pattern $\{\bar{n}_m(\delta)\}$ with the superposition of the classical mean fields, as given in Eqs. (32) and (33), arises for the pair of fields with a definite relative phase, which originate in a common U(1)-invariant source $\hat{\rho}_1^{\mathrm{com}}$ through a unitary transformation in Eq. (8). This is understood by noting the relation from Eq. (23),

$$\hat{\Psi}_m^\dagger \hat{\Psi}_m = (\phi_{ma}^* \hat{a}^\dagger + \phi_{mb}^* \hat{b}^\dagger)(\phi_{ma}\hat{a} + \phi_{mb}\hat{b}) = \left|c\phi_{ma} + e^{i\delta} s \phi_{mb}\right|^2 \hat{c}_1^\dagger \hat{c}_1 + \cdots, \quad (55)$$

up to the irrelevant terms involving the vacuum mode $\hat{c}_2$. The mean photon count at each detector is given by

$$\langle n_m \rangle_{\mathrm{com}} = \mathrm{Tr}[\hat{\rho}_1^{\mathrm{com}} \otimes (|0\rangle\langle 0|)_2 \hat{I}_m] = \bar{n}_m(\delta), \quad (56)$$

where $\alpha = c\sqrt{\bar{N}}$ and $\beta = e^{i\delta} s\sqrt{\bar{N}}$ in Eq. (33) with the mean photon number of the common source $\bar{N} = \mathrm{Tr}[\hat{\rho}_1^{\mathrm{com}} \hat{c}_1^\dagger \hat{c}_1]$. The shot noise Δn_m is also given [2] by

$$(\Delta n_m)^2 = \langle : (\hat{I}_m)^2 : \rangle + \langle \hat{I}_m \rangle - (\langle \hat{I}_m \rangle)^2 = (\bar{n}_m)^2 (\Delta N/\bar{N})^2 + \bar{n}_m[1 - (\bar{n}_m/\bar{N})], \quad (57)$$

which is determined by the statistics of the common source $\hat{\rho}_1^{\mathrm{com}}$. Hence, for a super-Poissonian $\hat{\rho}_1^{\mathrm{com}}$ with $\Delta N \sim \bar{N}$ such as a thermal state, the interference pattern is not observed practically in a single run of measurement due to the large shot noise. It may rather appear by accumulating the outcomes of many runs keeping the definite relative phase. This is in contrast with the case of independent super-Poissonian sources, where the interference pattern does not arise anyway due to the random relative phases run by run.

The mean-field description for the interference pattern $\{\bar{n}_m(\delta)\}$ in Eq. (32) is similarly applicable to the case of the two source fields $\hat{\rho}_{ab}(\delta)$ with a definite relative phase δ in Eq. (11) by sharing the common reference frame. The shot noise is determined depending on the source field statistics.

V. NUMERICAL ANALYSIS

We here present detailed numerical calculations on the probability distributions of the photon counts for a variety of independent U(1)-invariant source fields. This analysis confirms the features of the single-shot interference in terms of the mean-field description, which have been examined so far. We show specifically the behavior of the joint probabilities $P(n_1, n_2)$ and $P(n_1, n_2, n_3)$ for two and three detectors, together with their conditional distributions $P^{\mathrm{c}}(n_2|n_1)$ and $P^{\mathrm{c}}(n_3|n_1, n_2)$.

A. Poissonian sources

As the prototype, we first present the results for the Poissonian sources $\hat{\Pi}_a \otimes \hat{\Pi}_b$, which provide the essential

understandings how an interference pattern appears in each shot according to the probability distribution of photon detection. The detector matrices $R^{(m)}$ $(m = 1, 2, 3)$ in Eqs. (19) and (20) are chosen typically as

$$\begin{aligned} &R^{(1)}_{aa} = 0.3, \quad R^{(1)}_{bb} = 0.2, \quad \xi_1 = 1, \quad \theta_1 = 0; \\ &R^{(2)}_{aa} = 0.2, \quad R^{(2)}_{bb} = 0.3, \quad \xi_2 = 1, \quad \theta_2 = 0.7\pi; \\ &R^{(3)}_{aa} = 0.2, \quad R^{(3)}_{bb} = 0.3, \quad \xi_3 = 1, \quad \theta_3 = -0.5\pi. \end{aligned} \tag{58}$$

The mean photon numbers of the Poissonian sources $\hat{\Pi}_a \otimes \hat{\Pi}_b$ are taken as

$$\bar{N}_a = \bar{N}_b = 500, \tag{59}$$

which provide the mean photon counts at the detectors in Eq. (24),

$$\{\langle n_1\rangle, \langle n_2\rangle, \langle n_3\rangle\} = \{250, 250, 250\}. \tag{60}$$

The probability distribution $P(n_1)$ of the photon count n_1 at detector 1 is plotted in Fig. 2, which is given by

$$P(n_1) = \sum_{n_2 \cdots n_M} P(\mathbf{n}_M) = \int_{-\pi}^{\pi} \frac{d\delta}{2\pi} P(n_1; \delta). \tag{61}$$

This distribution appears roughly flat for $0 \lesssim n_1 \lesssim 2\langle n_1\rangle = 500$, corresponding to the range of $\bar{n}_1(\delta)$ for $-\pi \le \delta < \pi$, as the Poisson distribution $P(n_1; \delta)$ in the mean-field description is averaged over the intrinsically unknown relative phase δ. It represents roughly the overview of the peak manifold of $P(\mathbf{n}_M)$ along the n_1 axis. The squeezed peak of $P(n_1, n_2)$ corresponding to $\bar{n}_2(\delta_2) \ll \langle n_2\rangle$ in Fig. 1 is smoothed out for $P(n_1)$ by taking the sum over n_2, while that corresponding to $\bar{n}_1(\delta_1) \ll \langle n_1\rangle$ is still seen around $n_1 \approx 0$. It is also noticed that $P(n_1)$ is enhanced around $n_1 \approx \bar{n}_1(\delta)_{\max}$ $(\approx 2\langle n_1\rangle = 500)$. This is because the peak manifold of $P(n_1, n_2)$ appears somewhat thicker there along the n_2 axis, which is tangent to the mean-field trajectory.

The conditional distribution $P^{\rm c}(n_2|n_1)$ is plotted in Fig. 3. Here, the first outcome is set, for example, as $n_1 = \bar{n}_1(\delta) = 106$, which corresponds to the mean-field values $\bar{n}_2^+ \approx 174$ with $\delta^+(n_1) = +0.7\pi$ and $\bar{n}_2^- \approx 495$ with $\delta^-(n_1) = -0.7\pi$, as indicated with the vertical dotted lines. The relevant Poisson distributions $C_+P(n_2; \delta^+)$ and $C_-P(n_2; \delta^-)$ with $C_\pm = 1/2$ are shown together, as suggested in Eq. (45). The distribution around $\bar{n}_2^- \approx 495$ is in good agreement with $P(n_2; \delta^-)/2$, while that around $\bar{n}_2^+ \approx 174$ is slightly broader than $P(n_2; \delta^+)/2$. This is due to the uncertainty in the estimation of the relative phase δ with the smaller $\bar{n}_2^+$.

The conditional distributions $P^{\rm c}(n_3|n_1, n_2)$ are plotted in Fig. 4, where the mean-field values are taken as the outcomes, $(n_1, n_2) = (\bar{n}_1 = 106, \bar{n}_2^+ \approx 174)$ and $(\bar{n}_1 = 106, \bar{n}_2^- \approx 495)$, respectively, for $\delta^+ = +0.7\pi$ and $\delta^- = -0.7\pi$. They essentially agree with the relevant Poisson distributions $P(n_3; \delta^+)$ and $P(n_3; \delta^-)$, as suggested in Eq. (46), though slightly broader in the case of δ^- due to the uncertainty of the relative phase for the smaller $n_3 \approx \bar{n}_3^-$. The mean-field values $\bar{n}_3^+ \approx 448$ and $\bar{n}_3^- \approx 52$ are indicated with the vertical dotted lines.

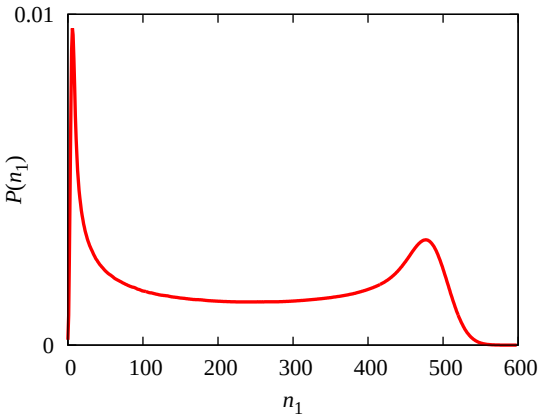

FIG. 2. (Color online) The probability distribution $P(n_1)$ of the photon count n_1 at detector 1 is plotted for the Poissonian sources $\hat{\Pi}_a \otimes \hat{\Pi}_b$ with $\bar{N}_a = \bar{N}_b = 500$. This distribution appears roughly flat for $0 \lesssim n_1 \lesssim 2\langle n_1\rangle = 500$, corresponding to the range of $\bar{n}_1(\delta)$ for $-\pi \le \delta < \pi$, as the Poisson distribution $P(n_1; \delta)$ in the mean-field description is averaged over the unknown relative phase δ.

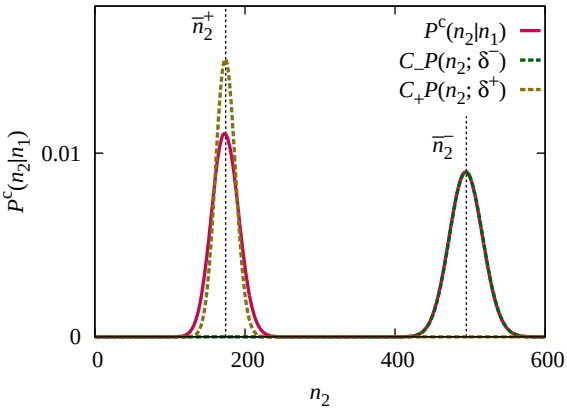

FIG. 3. (Color online) The conditional distribution $P^{\rm c}(n_2|n_1)$ (the solid line) is plotted for the Poissonian sources $\hat{\Pi}_a \otimes \hat{\Pi}_b$ with $\bar{N}_a = \bar{N}_b = 500$. It is compared with the relevant Poisson distributions $C_+P(n_2; \delta^+)$ (the left dashed line) and $C_-P(n_2; \delta^-)$ (the right dashed line) with $C_\pm = 1/2$, as suggested in Eq. (45). The mean-field values $\bar{n}_2^+ \approx 174$ and $\bar{n}_2^- \approx 495$ for $n_1 = 106$ are indicated with the vertical dotted lines.

These results of $P(n_1)$, $P^{\rm c}(n_2|n_1)$ and $P^{\rm c}(n_3|n_1, n_2)$ really indicate the existence of the peak manifold of $P(\mathbf{n}_M)$ along the mean-field trajectory. This is overlooked in Fig. 1 for the joint probability $P(n_1, n_2)$. The feature of the joint probability $P(n_1, n_2, n_3)$ of the three detector counts (n_1, n_2, n_3) is also depicted in Fig. 5. Here, the points providing significant prob-

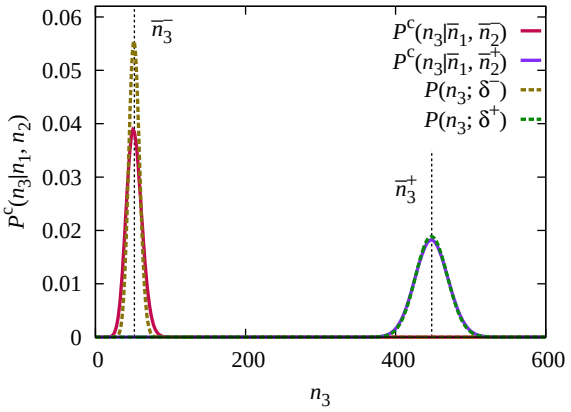

FIG. 4. (Color online) The conditional distributions $P^c(n_3|n_1,n_2)$ (the solid lines) are plotted for the Poissonian sources $\hat{\Pi}_a \otimes \hat{\Pi}_b$ with $\bar{N}_a = \bar{N}_b = 500$, where the mean-field values are taken as the outcomes, $(n_1,n_2) = (\bar{n}_1 = 106, \bar{n}_2^+ \approx 174)$ and $(\bar{n}_1 = 106, \bar{n}_2^- \approx 495)$, respectively, for $\delta^+ = +0.7\pi$ and $\delta^- = -0.7\pi$. They are compared with the relevant Poisson distributions $P(n_3;\delta^+)$ (the right dashed line) and $P(n_3;\delta^-)$ (the left dashed line), as suggested in Eq. (46). The mean-field values $\bar{n}_3^+ \approx 448$ and $\bar{n}_3^- \approx 52$ are indicated with the vertical dotted lines.

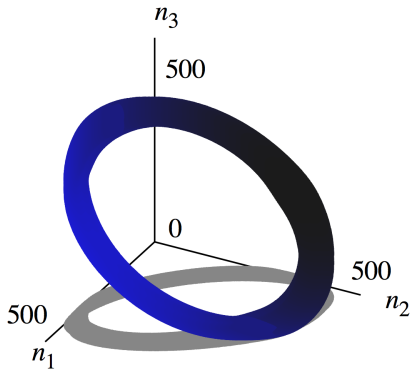

FIG. 5. (Color online) The joint probability $P(n_1,n_2,n_3)$ is depicted in the (n_1,n_2,n_3) space for the Poissonian sources $\hat{\Pi}_a \otimes \hat{\Pi}_b$ with $\bar{N}_a = \bar{N}_b = 500$. Here, the points providing significant probabilities above a certain threshold value $P_{\min}$ (numerically 1.6×10^{-7}) are plotted as dots to exhibit the peak manifold (blue) along the mean-field trajectory $\{\bar{n}_1(\delta), \bar{n}_2(\delta), \bar{n}_3(\delta)\}$ $(-\pi \le \delta < \pi)$, together with its projection (gray) on the (n_1,n_2) plane along $\{\bar{n}_1(\delta), \bar{n}_2(\delta)\}$. Each of these points is realized as a single-shot interference pattern.

abilities, $P(n_1,n_2,n_3) \ge P_{\min}$, are plotted as dots to exhibit the peak manifold along the mean-field trajectory $\{\bar{n}_1(\delta), \bar{n}_2(\delta), \bar{n}_3(\delta)\}$ $(-\pi \le \delta < \pi)$, together with its projection on the (n_1,n_2) plane along $\{\bar{n}_1(\delta), \bar{n}_2(\delta)\}$. Each of these points is realized as a single-shot interference pattern. The threshold value of the probability may be chosen suitably as $P_{\min} \sim 0.1\bar{P} \sim 0.01/\bar{n}^2$ with $2\pi\bar{n} \times \sqrt{\bar{n}} \times \sqrt{\bar{n}} \times \bar{P} = 1$ and $\bar{n} = (\langle n_1\rangle + \langle n_2\rangle + \langle n_3\rangle)/3$; numerically $P_{\min} = 1.6 \times 10^{-7}$ here. This calculation of $P(n_1,n_2,n_3)$ in the (n_1,n_2,n_3) space actually provides the simulation of interference experiments for the three detectors.

B. Sub-Poissonian sources

As a typical sub-Poissonian case, consider the binomial state involving the scaling parameter q (rational) with a fixed mean photon number $\bar{N}$ as

$$\hat{B}(q;\bar{N}) = \sum_{N=0}^{\bar{N}/q} B_N^{\bar{N}/q}(q)|N\rangle\langle N|. \tag{62}$$

Then, we have a sequence of the sub-Poissonian states for $0 < q \le 1$,

$$\hat{B}(q=1) = |\bar{N}\rangle\langle\bar{N}| \to \hat{B}(q) \to \hat{B}(q\to 0) = \hat{\Pi}. \tag{63}$$

The conditional distributions $P^c(n_2|n_1)$ with $n_1 = 42$ are plotted in Fig. 6 for the binomial sources $\hat{B}_a(q) \otimes \hat{B}_b(q)$ with $\bar{N}_{a,b} = \bar{N} = 200$ and some rational values of $q = \bar{N}/\bar{N}'$. Here, the detector matrices $R^{(m)}$ are taken the same as in Eq. (58) for the analysis of the Poissonian sources, while the mean photon number $\bar{N}$ is somewhat smaller due to the actual limitation for numerical computation. This sequence reproduces equivalently the probability distributions for the number-state sources $|\bar{N}',\bar{N}'\rangle = |\bar{N}/q, \bar{N}/q\rangle$ under the q-scaling in Eq. (28) with $R^{(m)\prime} = qR^{(m)}$ and $N_{a,b} = \bar{N}' = \bar{N}/q$, keeping $R^{(m)\prime}\bar{N}' = R^{(m)}\bar{N}$:

$$P_{\hat{B}(q)}(\mathbf{n}_M; R^{(m)}\bar{N}) = P_{\hat{N}}(\mathbf{n}_M; R^{(m)\prime}\bar{N}'). \tag{64}$$

Furthermore, we can see in Fig. 6 that in the limit $q \to 0$ the probability distribution for the binomial sources $\hat{B}_a(q) \otimes \hat{B}_b(q)$ approaches that for the Poissonian sources $\hat{\Pi}_a \otimes \hat{\Pi}_b$. On the other hand, under the q-scaling the Poissonian form of statistics is preserved, and the probability distribution is invariant. These observations indicate the relation

$$\begin{aligned} P_{\hat{B}(q\to 0)}(\mathbf{n}_M; R^{(m)}\bar{N}) &= P_{\hat{\Pi}}(\mathbf{n}_M; R^{(m)}\bar{N}) \\ &= P_{\hat{\Pi}}(\mathbf{n}_M; R^{(m)\prime}\bar{N}'). \end{aligned} \tag{65}$$

In the measurement of interference fringes with continuously distributed M detectors, the scaling parameter may be taken as $q = 1/M$ for the resolution. Then, by combining Eqs. (64) and (65) we find that for $q \to 0$ $(M \gg 1)$ the number-state sources $|\bar{N}',\bar{N}'\rangle$ and the Poissonian sources $\hat{\Pi}_a \otimes \hat{\Pi}_b$ with the sufficiently large $\bar{N}' = \bar{N}/q \to \infty$ provide essentially the same result of interference with fine spatial resolution as $R^{(m)\prime} = qR^{(m)} \to 0$. By a similar argument, this is also the case for the binomial sources $\hat{B}_a(q'';\bar{N}'') \otimes \hat{B}_b(q'';\bar{N}'')$ with any rational q'' and $\bar{N}'' = (q''/q)\bar{N} \to \infty$ as $R^{(m)\prime\prime} = (q/q'')R^{(m)} \to 0$.

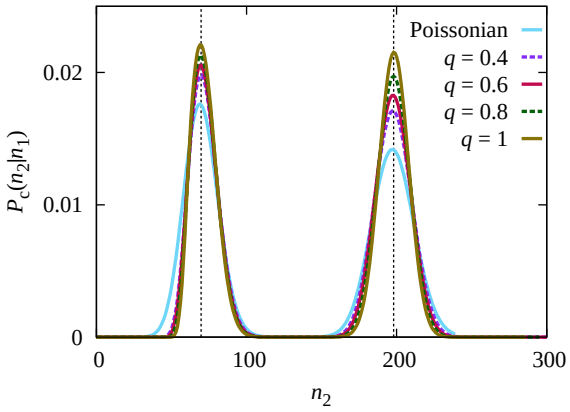

FIG. 6. (Color online) The conditional distributions $P^{\rm c}(n_2|n_1)$ with $n_1 = 42$ are plotted for the sub-Poissonian binomial sources $\hat{B}_a(q) \otimes \hat{B}_b(q)$ with $\bar{N}_{a,b} = \bar{N} = 200$ and some rational values of $q = \bar{N}/\bar{N}'$ corresponding to the sequence $|\bar{N}\rangle\langle\bar{N}|(q = 1) \to \hat{B}(q) \to \hat{\Pi}(q \to 0)$. The mean-field values $\bar{n}_2^+ \approx 70$ and $\bar{n}_2^- \approx 198$ for $n_1 = 42$ are indicated with the vertical dotted lines. This sequence reproduces equivalently the probability distributions for the number-state sources $|\bar{N}/q, \bar{N}/q\rangle$ under the q-scaling with $R^{(m)\prime} = qR^{(m)}$ and $\bar{N}' = \bar{N}/q$, keeping $R^{(m)\prime}\bar{N}' = R^{(m)}\bar{N}$.

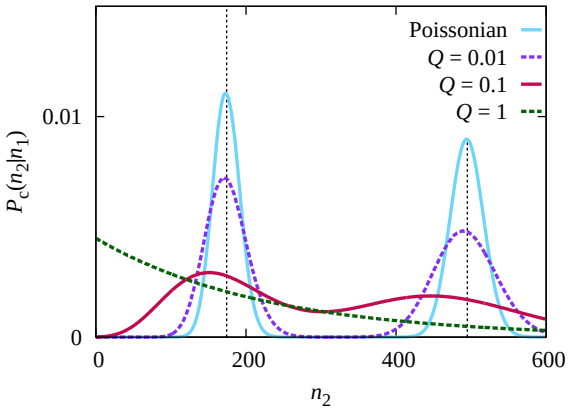

FIG. 7. (Color online) The conditional distributions $P^{\rm c}(n_2|n_1)$ with $n_1 = 106$ are plotted for a sequence of super-Poissonian sources given by $\mathcal{P}(|\alpha|; Q)$ in Eq. (66) with $\bar{N}_a = \bar{N}_b = 500$ and some values of Q. The mean-field values $\bar{n}_2^+ \approx 174$ and $\bar{n}_2^- \approx 495$ for $n_1 = 106$ are indicated with the vertical dotted lines.

C. Super-Poissonian sources

We have also considered a sequence of super-Poissonian states given by a U(1)-invariant form of coherent-state representation as

$$\mathcal{P}(|\alpha|; Q) \propto (|\alpha|^2/Q\bar{N})^{1/Q-1} \exp(-|\alpha|^2/Q\bar{N}), \qquad (66)$$

with the variance V depending on the parameter $Q > 0$,

$$V = \bar{N} + Q\bar{N}^2. \qquad (67)$$

The limit $Q \to 0$ corresponds to the Poissonian state $\hat{\Pi}$, whereas the case $Q = 1$ provides the thermal state $\hat{\Theta}$. The conditional distributions $P^{\rm c}(n_2|n_1)$ with $n_1 = 106$ are plotted in Fig. 7 for some values of Q, where $R^{(m)}$ and $\bar{N}_{a,b}$ are taken the same as in Eqs. (58) and (59) for the analysis of the Poissonian sources. The increasing variance V with Q broadens the distribution, as expected, eventually washing out the peak manifold for $Q \to 1$. Hence, the mean-field description is likely invalidated for super-Poissonian sources with rather broad distributions.

VI. CONCLUSION

In conclusion, we have investigated the interference of optical fields comprehensively under various configurations for sources and detectors. We have examined the probability distribution of photon detection to elucidate the quantum theoretical reasoning for the usual description of interference patterns with superposition of classical mean fields. Especially, for interference of two independent mixtures of number states with Poissonian or sub-Poissonian statistics, despite lack of intrinsic phases, it has been found that the joint probability of the photon counts at the detectors has a distinct peak manifold along the trajectory of the mean-field values with the varying relative phase. Then, the interference patterns should mostly be observed shot by shot as randomly chosen points in the peak manifold, specifying the values of the relative phase a posteriori. On the other hand, for super-Poissonian sources the mean-field description is likely invalidated with rather broad probability distributions.

ACKNOWLEDGMENTS

T. K. was supported by the JSPS Grant No. 22.1355.

Appendix A: Derivation of the joint probability

We present a derivation of the joint probability in Eq. (16), according to Refs. [15–18]. The probability that $n_1, \ldots, n_M$ photoelectrons are emitted from the respective surfaces $S_1, \ldots, S_M$ in the time interval T is represented [15, 18] as

$$P(n_1, \ldots, n_M) = \prod_{m=1}^{M} \frac{1}{n_m!} \frac{\partial^{n_m}}{\partial z_m^{n_m}} F(z_1, \ldots, z_M) \Big|_{z_m=-1}, \qquad (A1)$$

with the generating function

$$F(z_1,\ldots,z_M) \equiv \sum_{n_1,\ldots,n_M} P(n_1,\ldots,n_M) \prod_{m=1}^{M} (1+z_m)^{n_m}. \tag{A2}$$

This generating function can be expressed in terms of the joint probability $w_k(m_1,t_1;\ldots;m_k,t_k)dt_1\cdots dt_k$ that the k photoionizations occur, respectively, at S_{m_j} in the interval t_j to t_j+dt $(j=1,\ldots,k)$ [15]:

$$F(z_1,\ldots,z_M) = \sum_{k=0}^{\infty} \frac{1}{k!} \sum_{m_1,\ldots,m_k=1}^{M} z_{m_1}\cdots z_{m_k} \times \int_0^T w_k(m_1,t_1;\ldots;m_k,t_k)dt_1\cdots dt_k. \tag{A3}$$

A quantum-mechanical expression for w_k is derived phenomenologically for the narrow-band field propagating in the $+z$ direction [17] as

$$w_k(m_1,t_1;\ldots;m_k,t_k) = \eta_{m_1}\cdots\eta_{m_k} \int_{S_{m_1}} dx_1dy_1\cdots\int_{S_{m_k}} dx_kdy_k \times \mathrm{Tr}\left[:\prod_{l=1}^{k} \hat{\psi}^\dagger(\mathbf{x}_l,t_l)\hat{\psi}(\mathbf{x}_l,t_l):\right], \tag{A4}$$

where η_m is the quantum efficiency $(0<\eta_m\le 1)$, and the positive-frequency field operator $\hat{\psi}$ is given in Eq. (1). By substituting Eq. (A4) into Eq. (A3) for the generating function, the expression in Eq. (16) for the joint probability $P(n_1,\ldots,n_M)$ is obtained in terms of the photon-flux operators $\hat{I}_m$ in Eq. (13). Note here that Eq. (13) coincides with Eq. (17) in Ref. [16] for the linearly polarized optical field under the paraxial approximation, which represents the number of photons that cross the surface S_m in the time interval T.

[1] R. J. Glauber, Phys. Rev. **130**, 2529 (1963).
[2] L. Mandel and E. Wolf, Rev. Mod. Phys. **37**, 231 (1965).
[3] G. Magyar and L. Mandel, Nature **198**, 255 (1963).
[4] R. L. Pfleegor and L. Mandel, Phys. Rev. **159**, 1084 (1967).
[5] H. Paul, Rev. Mod. Phys. **58**, 209 (1986).
[6] M. R. Andrews, C. G. Townsend, H.-J. Miesner, D. S. Durfee, D. M. Kurn, and W. Ketterle, Science **275**, 637 (1997).
[7] M. Naraschewski, H. Wallis, A. Schenzle, J. I. Cirac, and P. Zoller, Phys. Rev. A **54**, 2185 (1996).
[8] A. J. Leggett, *Quantum liquids: Bose condensation and Cooper pairing in condensed-matter systems* (Oxford University Press, New York, 2006).
[9] K. Mølmer, Phys. Rev. A **55**, 3195 (1997).
[10] B. C. Sanders, S. D. Bartlett, T. Rudolph, and P. L. Knight Phys. Rev. A **68**, 042329 (2003).
[11] S. D. Bartlett, T. Rudolph, and R. W. Spekkens, Rev. Mod. Phys. **79**, 555 (2007).
[12] J. Javanainen and S. M. Yoo, Phys. Rev. Lett. **76**, 161 (1996).
[13] F. Laloë, Eur. Phys. J. D **33**, 87 (2005); W. J. Mullin, R. Krotkov, and F. Laloë, Am. J. Phys. **74**, 880 (2006).
[14] M. Iazzi and K. Yuasa, Phys. Rev. A **83**, 033611 (2011).
[15] P. Kelley and W. Kleiner, Phys. Rev. **136**, A316 (1964).
[16] R. J. Cook, Phys. Rev. A **25**, 2164 (1982).
[17] R. S. Bondurant, Phys. Rev. A **32**, 2797 (1985).
[18] W. Vogel and D.-G. Welsch, *Quantum Optics* (Wiley-VCH, Berlin, 2006), Chap. 6.
[19] D. T. Pegg, Phys. Rev. A **79**, 053837 (2009).